Structure and Properties of Tris[bis(ethylenedithio)tetrathiafulvalenium]tetrachlorocopper(II) Hydrate, $(BEDT\text{-}TTF)_3CuCl_4\cdot H_2O$: First Evidence for Coexistence of Localized and Conduction Electrons in a Metallic Charge-Transfer Salt

P. Day,*,† M. Kurmoo,† T. Mallah,† I. R. Marsden,‡ R. H. Friend,‡ F. L. Pratt,§ W. Hayes,§ D. Chasseau,∥ J. Gaultier,∥ G. Bravic,∥ and L. Ducasse⊥

Contribution from The Royal Institution of Great Britain, 21 Albemarle Street, London W1X 4BS, U.K., Cavendish Laboratory, Madingley Road, Cambridge CB3 0HE, U.K., Clarendon Laboratory, Parks Road, Oxford OX1 3PU, U.K., and Laboratoire de Cristallographie et de Physique Cristalline, UA144 CNRS, and Laboratoire de Physico-Chimie Théorique, URA CNRS 503, Université de Bordeaux I, 351 Cours de la Libération, 33405 Talence Cedex, France. *Received April 22, 1992*

Abstract: The synthesis and physical characterization of a complex of BEDT-TTF [bis(ethylenedithio)tetrathiafulvalenium] with $Cu^{II}Cl_4^{2-}$ are reported. The structure of $(BEDT\text{-}TTF)_3CuCl_4\cdot H_2O$ (I) (crystal data: triclinic, space group $P\bar{1}$, a = 16.634 Å, b = 16.225 Å, c = 8.980 Å, α = 90.72°, β = 93.24°, γ = 96.76°, V = 2402 Å^3, Z = 2) consists of alternating layers of organic cations and inorganic anions. The organic layers contain three crystallographically independent molecules, each $^2/_3+$, and two distinct stacks alternating with each other. The anion is dimerized as $[CuCl_4\cdot H_2O]_2$, with the Cu^{II} in a distorted tetrahedral geometry. I is metallic down to 200 mK with a conductivity anisotropy at 300 K of 7:1 ($(\sigma \parallel a\text{-}c):(\sigma \perp a\text{-}c)$ = 140:20 S cm^{-1}) within the layers and an EPR spectrum characterized by two lines, one from each spin system (conduction and Cu^{2+} localized moments). The g value of the Cu resonance ($g_\parallel$ = 2.29 and $g_\perp$ = 2.05) decreases at a gradient of -4×10^{-5} K^{-1} from 4 to 300 K, while that of the conduction electron (g = 2.03–2.05) is temperature independent. The EPR line width increases by 25% and 90% for the Cu and the conduction electrons, respectively, over the same temperature range. The spin susceptibility derived from the Cu resonance fits to a Curie–Weiss law ($\Theta \approx 1$ (1) K) or to a Bleaney–Bowers model for a dimer ($J \approx 4$ (1) K), and that of the free carriers shows a Pauli type temperature-independent behavior between 30 and 300 K. Below 30 K, the intensity of the free-carrier resonance falls to 30% of the room-temperature value. From the EPR, there is indication of weak interaction between the two spin systems. From the optical reflectivity data, the width of the conduction band is estimated to be 0.6 eV. A band-structure calculation indicates several zero-transfer integrals, and the Fermi surface has very anisotropic pockets of both electrons and holes, suggesting a semi-metal.

Superconductivity and long-range magnetic ordering are two different cooperatively ordered states whose coexistence in the same material leads to numerous interesting phenomena.[1] The search for coexisting superconductivity and magnetic order has been pursued most vigorously up to now among ternary compounds; 15 classes of such compounds have been discovered, in five of which both superconductivity and long-range magnetic order have been found with certainty, for example, among borides, $(RE)T_4B_4$ (RE = rare earth; T = Rh, Ir), chalcogenides, $(RE)Mo_6X_8$ (X = S, Se), silicides, $(RE)_2T_3Si_5$ (T = Fe, Co), stannides, $(RE)T_xSn_y$ (T = Rh, Os), and phosphides, TiRuP. Most recently, high-T_c superconductors (for example, $ErBa_2Cu_3O_{7-x}$, $T_c \sim 90$ K) have been observed to order antiferromagnetically without destroying the superconducting state.[2] Most of the rare earth ternary compounds have ordered sublattices of magnetic RE ions and show superconductivity combined with long-range antiferromagnetic order. In those that order ferromagnetically, the appearance of long-range order is accompanied by the destruction of superconductivity, at the re-entrant temperature T_{c2}.

All the systems mentioned above contain continuous lattices, and the magnetic and conducting sublattices are independent of each other. To date, analogous systems are unknown among low-dimensional molecular conductors. However, the latter show several forms of magnetic order. For example, the organic conductor $(TMTSF)_2PF_6$ (TMTSF = tetramethyltetraselenafulvalenium) exhibits itinerant magnetism with a spin density wave (SDW) at 10 K.[3] The latter compound is metallic down to 10 K, but below this temperature, an energy gap opens at the Fermi surface due to the SDW. This transition is suppressed by pressure, and at 8 kbar, a superconducting ground state is established. On the other hand, when samples of $(TMTSF)_2ClO_4$ are slowly cooled at ambient pressure, a superconducting ground state is observed at ca. 1.5 K, while for rapidly cooled samples, a SDW state is observed in the temperature range $1 < T < 5.5$ K and superconductivity occurs below 1 K. Coexistence of SDW and superconductivity has not been proven.

The TMTSF salts are quite one-dimensional in character. However, in the two-dimensional layered salts of BEDT-TTF, several competing states are also found.[3] For example, superconducting, metallic, and semiconducting, as well as Pauli paramagnetic, 1D or 2D antiferromagnetic, SDW, and spin Peierls states have all been observed. Most recently, the metallic salt $(BEDT\text{-}TTF)_2KHg(SCN)_4$, which has an antiferromagnetic ground state below 10 K in low field,[4] was inferred to have a ferromagnetic character in fields above 22 T.[5]

† Royal Institution.
‡ Cavendish Laboratory.
§ Clarendon Laboratory.
∥ Laboratoire de Cristallographie et de Physique Cristalline, Université de Bordeaux 1.
⊥ Laboratoire de Physico-Chimie Théorique, Université de Bordeaux 1.

(1) See for example: (a) *Superconductivity in Magnetic and Exotic Materials*; Matsubara, T., Kotani, A., Eds.; Springer Series in Solid State Sciences; Springer: Berlin, 1984; Vol. 52, pp 1–211. (b) *Superconductivity in Ternary Compounds*; Maple, M. B., Fischer, Ø., Eds.; Topics in Current Physics; Springer: Berlin, **1982**, Vol. 34, pp 1–292. (c) Bulaevskii, L. N.; Buzdin, A. I.; Kulic, M. L.; Panjukov, S. V. *Adv. Phys.* **1985**, *34*, 175–261.
(2) Hor, P. H.; Meng, R. L.; Wang, Y. Q. *Phys. Rev. Lett.* **1987**, *58*, 1891–1894.
(3) Proceedings of the International Conference on Synthetic Metals. *Synth. Met.* **1987**, *19*; **1989**, 27–29; **1991**, 41–43.
(4) Sasaki, T.; Toyota, N.; Tokumoto, M.; Kinoshita, N.; Anzai, H. *Solid State Commun.* **1990**, *75*, 93–96, 97–100.
(5) Pratt, F. L.; Doporto, M.; Singleton, J.; Janssen, T. J. B. M.; Perenboom, J. A. A. J.; Kurmoo, M.; Hayes, W.; Day, P. *Physica B* **1992**, *177*, 333–338; *Phys. Rev. B* **1992**, *45*, 13904–13912.

0002-7863/92/1514-10722$03.00/0

In the present paper, we adopt a novel approach to the study of interactions between free carriers and localized moments. Our aims are to tune the long-range magnetic order and to stabilize a superconducting state in a magnetically ordered molecular lattice.[6,7] The approach is to develop charge-transfer salts having magnetic moments on the anions.

We chose to investigate BEDT-TTF salts containing $CuCl_4^{2-}$ for two reasons: first, because a ferromagnetic ground state has been found in several Cu(II) salts with layered structures,[8] as well as the more common antiferromagnetic ones, and, second, because the EPR of Cu d^9 electrons is easily studied due to the dipole–dipole narrowing effects and the fact that it has one hole in an otherwise filled subshell.[9] Incorporation of magnetic ions into organic conductors has been successfully achieved in a few cases. For example, in Cu(pc)I, (pc is phthalocyanine), a molecular metal with a one-dimensional array of local moments embedded in a Fermi sea of charge carriers,[10] it has been shown by EPR and NMR that the principal magnetic interactions between Cu^{2+} moments arise from indirect exchange involving the conduction electrons.[10]

In this paper, we report the synthesis, the crystal and electronic structures, and the electrical-transport, magnetic, and optical properties of (BEDT-TTF)$_3$Cu^{II}Cl$_4$·H$_2$O (I). In this connection, we also review briefly the structures and properties of known BEDT-TTF salts containing magnetic anions, as well as compare the properties of the titled material with those having the same stoichiometry and approximately the same structure but containing nonmagnetic anions. Preliminary notes of the crystal structure and properties of I have been published.[6,7]

Experimental Section

Synthesis. BEDT-TTF was obtained by the method of ref 11 and recrystallized twice from chloroform. $[(CH_3)_4N]_2CuCl_4$ was synthesized by metathesis of equivalent amounts of $[(CH_3)_4N]Cl$ and $CuCl_2·6H_2O$ in absolute ethanol and recrystallized from ethanol just before use. Elemental analyses confirmed the purity of the materials. The charge-transfer salts were obtained by electrocrystallization of BEDT-TTF (50 mg) in either benzonitrile or a mixture of acetonitrile (10%) and dichloromethane (90%) saturated with $[(CH_3)_4N]_2CuCl_4$. All solvents were distilled before use. A three-compartment cell with platinum electrodes was used. The current was kept constant at 2 μA for at least 10 days. Two types of crystals were obtained: hexagonal plates, I, and multifaceted needles, (BEDT-TTF)$_2$CuCl$_4$.

The quality of crystals can vary widely depending on the amount of water present in the electrochemical crystal-growing cell. In addition to the two salts just mentioned, several byproducts can be obtained due to the fact that the $CuCl_4^{2-}$ ion is unstable in the presence of water and reacts to yield eventually $Cu(H_2O)_6^{2+}$ and Cl^-. The Cu^{2+} will oxidize BEDT-TTF, as we have shown previously,[12a] to give α′-(BEDT-TTF)$_2$Cu^{I}Cl$_2$, a Mott–Hubbard semiconductor (E_A = 0.3 eV) with a one-dimensional antiferromagnetic chain (J = 53 K). In the presence of chloride ions and water molecules, we have demonstrated that three types of crystals,[13] (BEDT-TTF)$_3$Cl$_2$·2H$_2$O, (BEDT-TTF)$_4$Cl$_2$·4H$_2$O, and (BEDT-TTF)$_4$Cl$_2$·6H$_2$O, can be obtained. They are all highly conducting at room temperature, with a semimetallic character and a very broad minimum in resistivity at ca. 150 K. The charge stoichiometry of (BEDT-TTF)$_3$Cl$_2$·2H$_2$O and its crystal structure are quite analogous to those of I. The modes of packing of the BEDT-TTF molecules within a layer are almost identical in the two materials. Although the volumes differ by 4% (2300 Å^3 for the chloride and 2402 Å^3 for I), it is conceivable that a solid solution of the chloride and I might occur. This may account for the difference in conductivity behavior of different crystals (see below), though it will not affect EPR measurements greatly as this technique probes localized Cu^{2+} ions and the conduction electrons irrespective of the small lattice defects that may accompany slight doping.

Table I. Crystal Data for I

formula	$C_{30}H_{26}S_{24}OCuCl_4$
a/Å	16.634 (4)
b/Å	16.225 (9)
c/Å	8.980 (3)
α/deg	90.72 (3)
β/deg	93.24 (3)
γ/deg	96.76 (3)
V/Å^3	2402 (1)
Z	2
T/K	295
space group	$P\bar{1}$
crystal size/mm^3	0.34 × 0.12 × 0.06
λ(Cu Kα)/Å	1.541 78
μ/cm^{-1}	122.36
$\theta/2\theta$ scan, θ_{max}/deg	71.5
scan width/deg	$\Delta\theta = 0.8 + 0.142 \tan\theta$
no. of data collected	9638
no. of unique data	9314
no. of unique data ($I > 3\sigma(I_o)$)	7266
no. of variables	541
R	0.050
R_w	0.053
$(\Delta/\sigma)_{max}$	0.04

X-ray Diffraction. A crystal of I (Table I) of dimensions 0.34 × 0.12 × 0.06 mm^3 was mounted on a Siemens AED four-circle diffractometer using Ni-filtered Cu Kα radiation (λ = 1.541 78 Å). Intensities of 9314 reflections were collected using the $\theta/2\theta$ scan technique (θ_{max} = 71.5°). Refined cell parameters were obtained from the setting angles of 11 reflections within 22 < θ < 60°. Three intensity standard reflections (18,−1,0; 5,−6,0; 12,−7,9) were monitored every 50 data collected. No significant variation was observed. The data were corrected for absorption, using a Gaussian integration procedure,[14] and for Lorentz and polarization effects. A total of 7266 reflections with $I > 3\sigma(I_o)$ were considered as observed. The structure was solved by direct methods using SIR88.[15] The positions of the heavy atoms (Cu, Cl, and S) were found, and the remainder were located by Fourier methods. The H atoms on the water molecules were observed from the difference maps, and those of the BEDT-TTF molecules were placed at idealized positions with fixed isotropic thermal parameters. Scattering factors, including terms for

(6) (a) Gudenko, A. V.; Ginodman, V. B.; Korotkov, V. E.; Koshelap, A. V.; Kushch, N. D.; Laukhin, V. N.; Rozenberg, L. P.; Khomenko, A. G.; Shibaeva, R. P.; Yagubskii, E. B. *The Physics and Chemistry of Organic Superconductors*; Saito, G., Kagoshima, S., Eds.; Springer Proceedings in Physics; Springer: Berlin, 1990; Vol. 51, pp 365–368. (b) After submission of the present paper for publication, a more extended report of the crystal structure of I appeared: Shibaeva, R. P.; Korotkov, V. E.; Rozenberg, L. P. *Sov. Phys.—Crystallogr. (Engl. Transl.)* **1991**, *36*, 820–824. The latter is in overall agreement with the structure reported here, though based on a smaller data set (5012 unique reflections with $I \geq 3\sigma(I)$) and a larger R factor (0.065).

(7) (a) Kurmoo, M.; Mallah, T.; Day, P.; Marsden, I.; Allan, M.; Friend, R. H.; Pratt, F. L.; Hayes, W.; Chasseau, D.; Gaultier, J.; Bravic, G. *The Physics and Chemistry of Organic Superconductors*; Saito, G., Kagoshima, S., Eds.; Springer Proceedings in Physics; Springer: Berlin, 1990; Vol. 51, pp 290–293. (b) Mallah, T.; Hollis, C.; Bott, S.; Day, P.; Kurmoo, M. *Synth. Met.* **1988**, *27*, A381–386. (c) Mallah, T.; Hollis, C.; Bott, S.; Kurmoo, M.; Day, P. *J. Chem. Soc., Dalton Trans.* **1990**, 859–865.

(8) See e.g.: Carlin, R. L. *Magnetochemistry*; Springer Verlag: Berlin, 1986; p 143.

(9) Abragam, A.; Bleaney, B. *Electron Paramagnetic Resonance of Transition Ions*; Clarendon Press: Oxford, U.K., 1970.

(10) (a) Ogawa, M. Y.; Martisen, J.; Palmer, S. M.; Stanton, J. L.; Tanaka, J.; Greene, R. L.; Hoffman, B. M.; Ibers, J. A. *J. Am. Chem. Soc.* **1987**, *109*, 1115–1121. (b) Ogawa, M. Y.; Hoffman, B. M.; Lee, S.; Yudkowsky, M.; Halperin, W. P. *Phys. Rev. Lett.* **1986**, *57*, 1177–1180. (c) Ogawa, M. Y.; Palmer, S. M.; Liou, K.; Quirion, G.; Thompson, J. A.; Poirier, M.; Hoffman, B. M. *Phys. Rev. B* **1989**, *39*, 10682–10692.

(11) (a) Larsen, J.; Lenoir, C. *Synthesis* **1988**, *2*, 134. (b) Wang, H. H.; Reed, P. E.; Williams, J. M. *Synth. Met.* **1986**, *14*, 165–172. (c) Geiser, W.; Wang, H. H.; Hammond, C. E.; Firestone, M. A.; Beno, M. A.; Carlson, K. D.; Numez, L.; Williams, J. M. *Acta Crystallogr.* **1987**, *C43*, 656.

(12) (a) Kurmoo, M.; Talham, D. R.; Day, P.; Howard, J. A. K.; Stringer, A. M.; Obertelli, D. S.; Friend, R. H. *Synth. Met.* **1988**, *22*, 415–418. (b) Bu, X.; Coppens, B.; Lederle, B.; Naughton, M. J. *Acta Crystallogr.* **1991**, *C47*, 2082–2085.

(13) (a) Kurmoo, M.; Rosseinsky, M. J.; Day, P.; Auban, P.; Kang, W.; Jerome, D.; Batail, P. *Synth. Met.* **1988**, *27*, A425–431. (b) Rosseinsky, M. J.; Kurmoo, M.; Talham, D. R.; Day, P.; Chasseau, D.; Watkin, D. *J. Chem. Soc., Chem. Commun.* **1988**, 88–90. (c) Mori, T.; Inokuchi, H. *Chem. Lett.* **1987**, 1657–1660. (d) Mori, T.; Inokuchi, H. *Solid State Commun.* **1987**, *64*, 335–337. (e) Obertelli, S. D.; Marsden, I. R.; Friend, R. H.; Kurmoo, M.; Rosseinsky, M. J.; Day, P.; Pratt, F. L.; Hayes, W. *The Physics and Chemistry of Organic Superconductors*; Saito, G., Kagoshima, S., Eds.; Springer Proceedings in Physics; Springer: Berlin, **1990**, Vol. 51, pp 181–184. (f) Bravic, G.; Chasseau, D.; Gaultier, J.; Rosseinsky, M. J.; Kurmoo, M.; Day, P.; Filhol, A. *Synth. Met.* **1991**, *41–43*, 2035–2038.

(14) Coppens, P.; Leiserowitz, L.; Rabinovitch, D. *Acta Crystallogr.* **1965**, *18*, 1035–1038.

(15) Burla, M. C.; Camalli, M.; Cascarano, G.; Giacovazzo, C.; Polidori, G.; Spagna, R.; Viterbo, D. *J. Appl. Crystallogr.* **1989**, *22*, 389–393.

Table II. Modes of Stacking Intermolecular S-S Distances (<3.9 Å) and Intermolecular Transfer Integrals (t) in I[a]

mode	molecules	atoms	S-S/Å	t/meV
		A Stacks		
A1	I ↔ I + a + b	S(12)-S(22)	3.76	2.47
A2	I ↔ I + a + b + c	shortest S-S	3.83	0
		B Stacks		
B1	II ↔ III	S(42)-S(51)	3.88	28.9
		S(44)-S(61)	3.84	
		S(44)-S(62)	3.81	
B2	II ↔ III + c	S(31)-S(52)	3.78	28.9
		S(41)-S(62)	3.78	
AB1	I ↔ II	S(13)-S(32)	3.40	-36.8
		S(13)-S(34)	3.34	
		S(21)-S(44)	3.53	
		S(23)-S(44)	3.42	
AB2	I ↔ II	S(12)-S(32)	3.78	98.7
		S(14)-S(42)	3.72	
		S(22)-S(34)	3.80	
		S(24)-S(34)	3.75	
AB3	I ↔ III	S(14)-S(62)	3.60	-32.9
		S(14)-S(64)	3.55	
		S(22)-S(54)	3.41	
		S(24)-S(54)	3.38	
AB4	I ↔ III	S(11)-S(54)	3.70	100.5
		S(23)-S(62)	3.76	
		S(23)-S(64)	3.61	
BB1	II ↔ III	S(33)-S(61)	3.44	-42.4
		S(41)-S(53)	3.32	
		S(43)-S(53)	3.42	
BB2	II ↔ II	S(31)-S(51)	3.78	64.2
		S(33)-S(43)	3.71	
BB3	III ↔ III	S(53)-S(61)	3.70	98.7

[a] Labeling of stacks and molecules is shown in Figure 3.

anomalous dispersion, were taken from ref 16. All non-H atoms were refined anisotropically using block-diagonal least-squares refinement based on F_o with weights of the form

$$\omega = \omega_o[1 + \omega_o(aF_o)^b]^{-1} \qquad \omega_o = [\sigma(F_o)^2/2|F_o|]^{-2}$$

The values of a and b were adjusted to 0.03 and 1.8, respectively, to obtain a flat variance distribution with F_o. Convergence to R = 0.050 (R_w = 0.053) was obtained using 541 variable parameters. A difference Fourier map calculated after final refinement was essentially featureless with maximum electron densities of ±0.3 eÅ^{-3}. Final values are S = 1.15 and $(\Delta/\sigma)_{max}$ = 0.04.

Charge-Transport Measurements. Temperature dependence of conductivity and thermopower over the range 2–350 K was measured by use of an Oxford Instruments CF200 continuous-flow cryostat. Conductivity measurements were performed on single crystals by both ac and dc methods. Contact to the crystals was made by gold wires attached to pre-evaporated gold pads with silver paint (gold paint for thermopower measurements) or directly to the crystal surface with platinum paint, in either the four-in-a-line or the Montgomery configuration. Pressure dependence of the conductivity was measured using a hydrostatic method employing a mixture of pentane and isopentane as described earlier.[17]

Electron Paramagnetic Resonance Measurements. Variable-temperature EPR spectra of single crystals were recorded using a Varian E9 X-band reflection spectrometer with a rectangular TE_{102} microwave cavity and an Oxford Instruments CF200 cryostat and temperature controller. Angular dependence of the EPR spectra was measured by use of a homemade goniometer. The single crystals were mounted with silicone grease on a Spectrosil quartz rod, which had been previously checked for magnetic impurities. Data were recorded both on an analog chart recorder and in digitized form for further analyses. The field was measured by a Hall-effect probe and calibrated using a diphenylpicrylhydrazyl (DPPH, g = 2.0037) marker. To take account of the Dysonian line shape,[18,19] each spectrum was fitted to the theoretical model for a flat-plate geometry sample. Several crystals were employed to check for sample dependence (and for other crystal phases). No variation was observed among different samples.

(16) *International Tables for X-ray Crystallography*; Kynoch Press: Birmingham, U.K., 1974; Vol. IV.
(17) Parker, I. D., Ph.D. Thesis, Cambridge University, 1988.
(18) Dyson, F. J. *Phys. Rev.* **1955**, *98*, 349–359.
(19) Feher, G.; Kip, A. F. *Phys. Rev.* **1955**, *98*, 337–348.

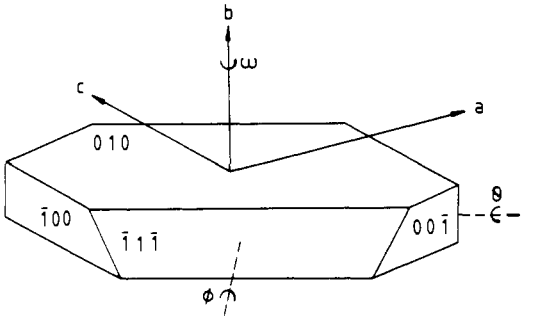

Figure 1. Crystal morphology of I, showing the labeling of the faces and the crystal orientation in the EPR rotation experiments.

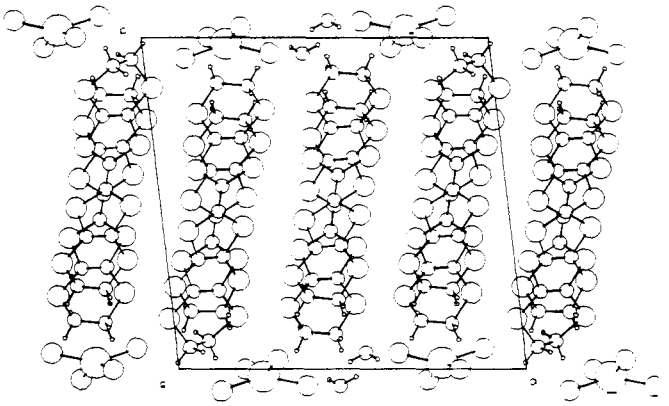

Figure 2. View of the unit cell of I along c.

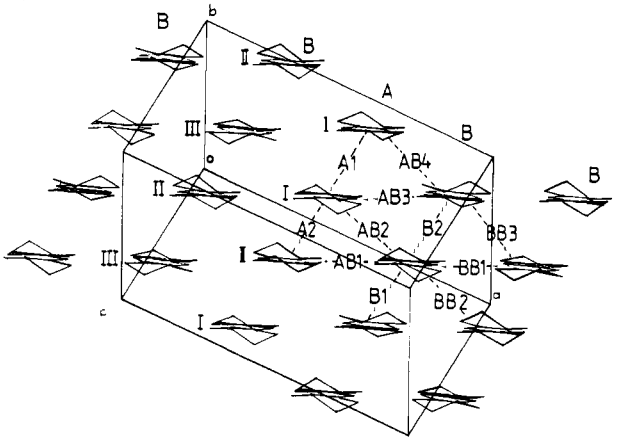

Figure 3. View of the 2D layer along the C=C bonds of the BEDT-TTF molecules in I, with the labeling of the transfer integrals employed in the band-structure calcualtion.

Optical Reflectivity Measurements. Two spectrometers were employed to record the reflectance spectra of the single crystals: a Perkin-Elmer 1710 (400–4300 cm^{-1}) and a Perkin-Elmer Lambda 9 (3000–50 000 cm^{-1}). The incident beam was focused on the samples or the reference gold or aluminum mirror. Spectra were obtained for two crystals. Both KRS5 and calcite polarizers were employed. All measurements were performed at room temperature.

Results

Crystal Structure of (BEDT-TTF)$_3$CuCl$_4$·H$_2$O (I). The atomic positional and thermal parameters arising from the structure determination of (BEDT-TTF)$_3$CuCl$_4$·H$_2$O (I) are given in Table A, and the bond lengths and angles, in Table B of the supplementary material. The intermolecular S–S contacts less than 3.9 Å are given in Table II.

The crystal belongs to the triclinic system $P\bar{1}$, with a = 16.634 Å, b = 16.225 Å, c = 8.980 Å, α = 90.72°, β = 93.24°, γ = 96.76°, V = 2402 Å^3, and Z = 2. The crystal morphology and labeling of the crystal faces are shown in Figure 1, and the labeling scheme of the atoms is shown in Figure A of the supplementary

material. The crystal structure consists of stacks of the organic donor BEDT-TTF parallel to the *c*-axis, with short interstack S–S contacts leading to the formation of layers in the *ac*-plane (Figure 2). These layers are interleaved by the inorganic anions and the water of crystallization. There are three crystallographically independent BEDT-TTF molecules (labeled I, II, and III in Figure 3) and two different stacks (labeled A and B). Stack A contains only BEDT-TTF of type I, and stack B has an alternate arrangement of II and III. Within the *ac*–layer, the stacks form an ABBABBA array (Figure 3). The anions lie in planes parallel to the layers of the donor, within which pairs of $CuCl_4$ anions are connected by hydrogen bonds through the two water molecules to form discrete units.

Since Cu can occur in any of three oxidation states and in principle any combination of these might exist within the same crystal, it is important to establish the exact oxidation state of the Cu atom as this determines the band filling of the conducting layers, and hence the shape of the Fermi surface and the transport properties. As the first step, we can gain some insight into the mean Cu oxidation state from the bond lengths of BEDT-TTF. Within this series of charge-transfer salts, there is an established correlation between the bond lengths and the formal charge on the BEDT-TTF molecules. First, it is reasonable to assume that the close similarity between the bond lengths of the central C=C bond of the three independent BEDT-TTF molecules in I indicates that they all carry the same charge. The average value of 1.363 (5) Å lies in the range of $(BEDT\text{-}TTF)^{1/2+}$ (1.35 Å,[12a] 1.361 Å[20]) and $(BEDT\text{-}TTF)^{2/3+}$ (1.38 Å,[13b] 1.37 Å[21]).

If the Cu atoms are divalent, then the latter is expected. For the former, the oxidation state of the Cu is required to be 2.5+, i.e. a mixed-valent material. Since the coordination geometries around all the Cu atoms in I are identical, such mixed valency would have to be class III type in the Robin–Day scheme.[22] Mixed valency of class II type has been invoked for (BEDT-TTF)$CuCl_2$[23a,b] and of class III type for (BEDT-TTF)$_3CuBr_3$.[23c–e] In both cases, the oxidation states of the Cu are 1+ and 2+; Cu^{III} halides are not known, apart from fluorides.[24]

The $CuCl_4$ moieties lie with the pseudo-4-fold axes perpendicular to the plane of the organic layers (Figure 2). The Cu–Cl bond lengths within the molecular complexes average 2.25 Å with a Cl–Cu–Cl angle of 150°. This coordination geometry is the most common for Cu^{II} halides, which are Jahn–Teller distorted. The Cu–Cl bond length is consistent with Cu^{II} distances; e.g., among Cu^{II} chlorides one finds for $Cu^{II}Cl_2·2H_2O$ 2.290 Å,[25] for $[(C_2H_5)_2NH_2]_2CuCl_4$ 2.254 Å,[26] and for $[(R_nH_{4-n})N]_2CuCl_4$ 2.252 Å,[27] while for Cu^{I} chlorides one finds for α'-(BEDT-TTF)$_2Cu^{I}Cl_2$ 2.086 Å,[12a] for β'-(BEDT-TTF)$_2Cu^{I}Cl_2$ 2.098 Å,[12b] and for $[(CH_3)_4N]Cu^{I}Cl_2$ 2.107 Å.[28] Thus, the C=C and Cu^{II}—Cl bond lengths, as well as the geometry of the anion, strongly suggest that the BEDT-TTF molecules are all $^2/_3$+. The two water molecules serve to bridge two $CuCl_4$ groups into a dimeric unit. The H···Cl distances are 2.34 and 2.63 Å. The distance between the two Cu atoms (Cu1···Cu2) of a pair in the unit cell is 8.761 (9) Å, and the nearest neighbor distances to those of adjacent unit cells are 8.98 (9) Å for Cu1···(Cu1 + *c*), 8.576 (1) Å for Cu2···(Cu1 + *a*), and 10.180 (1) Å for Cu2···(Cu1 + *a* + *c*).

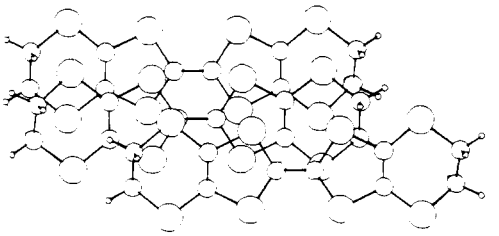

Figure 4. Mode of overlap of the BEDT-TTF molecules in I.

The bond lengths and angles of the three independent BEDT-TTF molecules are almost identical (see Table B of the supplementary material), except for the disorder of one of the $-CH_2CH_2-$ groups on molecule III. The thermal parameters of the latter carbon atoms are twice those of the others. The ethylene groups of the molecules I and II are all eclipsed. The two different modes of overlap of the BEDT-TTF molecules are the same in each of the two stacks (Figure 4). In addition, the molecules in both stacks form dimers, the mean interplanar distances defined by the four inner sulfur atoms in stack A being 3.58 and 3.74 Å and in stack B, 3.66 and 3.85 Å. Although at first sight these spacings appear to be quite different in the two stacks, in fact they are not because the mean planes defining the molecules are parallel in stack A but not in stack B; thus, the dihedral angle is 0° in stack A but 1.75° in stack B.

Band Structure of (BEDT-TTF)$_3$CuCl$_4$·H$_2$O (I). In principle, estimation of the intermolecular transfer integrals allows one to calculate the electronic band structure. However, the choice of approximation to be used in calculating the band structures of organic conductors is not straightforward. The most widely used method in recent years employs the tight-binding approximation in the context of a semiempirical extended Huckel theory (EHT).[29–31] Beyond this simple approach, only two attempts have been made to use the self-consistent-field ab-initio method.[32] However, the characteristics of the Fermi surface obtained by the EHT method generally agree well with the ones deduced experimentally from the Shubnikov–de Haas and de Haas–van Alphen oscillations in some representative salts of the β and κ phases of the BEDT-TTF salts.[33] For these reasons, the EHT approach has been retained in the calculation of the transfer integrals of I.

Within the EHT approach, in the metallic organic charge-transfer salts, the bands near the Fermi level are mainly built from the HOMO of the organic moiety.[30c] As the donor is nearly planar, the HOMO is of π-character, the molecular orbital being formed from the p_z atomic orbitals of the carbon and chalcogenide atoms. The tight-binding approximation can be used because the transfer integrals decrease very quickly with increasing intermolecular distance, so the gross features of the band structure of the charge-transfer salts may be accounted for by determining

(20) Kurmoo, M.; Talham, D. R.; Day, P.; Parker, I. D.; Friend, R. H.; Stringer, A. M.; Howard, J. A. K. *Solid State Commun.* **1987**, *61*, 459–464.
(21) Kobayashi, H.; Kato, R.; Mori, T.; Kobayashi, A.; Sasaki, Y.; Saito, G.; Enoki, T.; Inokuchi, H. *Chem. Lett.* **1984**, 179–182.
(22) Robin, M. B.; Day, P. *Adv. Inorg. Chem. Radiochem.* **1967**, *10*, 248–403.
(23) (a) Tanaka, M.; Kawamoto, A.; Tanaka, J.; Sano, M.; Enoki, T.; Inokuchi, H. *Bull. Chem. Soc. Jpn.* **1987**, *60*, 2531–2534. (b) Kawamoto, A.; Tanaka, J.; Tanaka, M. *Acta Crystallogr.* **1987**, *C43*, 205–207. (c) Kurmoo, M.; Kanazawa, D.; Day, P. In *Mixed-Valency Systems: Application to Chemistry, Physics and Biology*; Prassides, K., Ed.; NATO ARW Series, C343; Kluwer: 1991; pp 419–424. (d) Mori, T.; Sakai, T.; Saito, G.; Inokuchi, H. *Chem. Lett.* **1987**, 927–930. (e) Kurmoo, M.; Kanazawa, D.; Day, P. *Synth. Met.* **1991**, *41–43*, 2123–2126.
(24) Wells, A. F. *Structural Inorganic Chemistry*, 4th ed.; Oxford University Press: Oxford, U.K., 1975; p 877.
(25) Engberg, A. *Acta Chem. Scand.* **1970**, *24*, 3510–3526.
(26) (a) Simonsen, S. H.; Harlow, R. L. *Am. Crystallogr. Assoc. Abstr. Ser. 2* **1977**, *5*, HN5. (b) Halvorson, K. E.; Patterson, C.; Willett, R. D. *Acta Crystallogr.* **1990**, *B46*, 508–519 and references therein.
(27) (a) Clay, R.; Murray-Rust, J.; Murray-Rust, P. *Acta Crystallogr.* **1975**, *B31*, 289–290. (b) Smith, D. W. *Coord. Chem. Rev.* **1976**, *21*, 93–158.
(28) Apslund, M.; Jagner, S.; Nilsson, M. *Acta Chem. Scand.* **1983**, *A37*, 57–62.
(29) Hoffmann, R. J. *J. Chem. Phys.* **1963**, *39*, 1397–1412.
(30) (a) Whangbo, M.-H.; Walsh, W. M.; Haddon, R. C.; Wudl, F. *Solid State Commun.* **1982**, *43*, 637–639. (b) Mori, T. Ph.D. Thesis, Tokyo University, 1985. (c) Grant, P. M. *J. Phys., Collog.* **1983**, *44* (C3), 847–857.
(31) Ducasse, L.; Abderrabba, M.; Hoarau, J.; Pesquer, M.; Gallois, B.; Gaultier, J. *J. Phys. C: Solid State Phys.* **1986**, *19*, 3805–3820.
(32) (a) Kasowski, R. V.; Whangbo, M.-H. *Inorg. Chem.* **1990**, *29*, 360–362. (b) Kübler, J.; Weger, M.; Sommers, C. B. *Solid State Commun.* **1987**, *62*, 801–805.
(33) (a) Oshima, K.; Mori, T.; Inokuchi, H.; Urayama, H.; Yamochi, H.; Saito, G. *Phys. Rev.* **1988**, *B38*, 938–941. (b) Pratt, F. L.; Singleton, J.; Kurmoo, M.; Spermon, S. J. R. M.; Hayes, W.; Day, P. *The Physics and Chemistry of Organic Superconductors*; Saito, G., Kagoshima, S., Eds.; Springer Proceedings in Physics; Springer: Berlin, **1990**; Vol. 51, pp 200–203. (c) Kang, W.; Montambaux, G.; Cooper, J. R.; Jerome, D.; Batail, P.; Lenoir, C. *Phys. Rev. Lett.* **1989**, *62*, 2559–2562. (d) Heidmann, C.-P.; Müller, H.; Biberacher, W.; Neumaier, K.; Probst, Ch.; Andres, K.; Jansen, A. G. M.; Joss, W. *Synth. Met.* **1991**, *41–43*, 2029–2032.

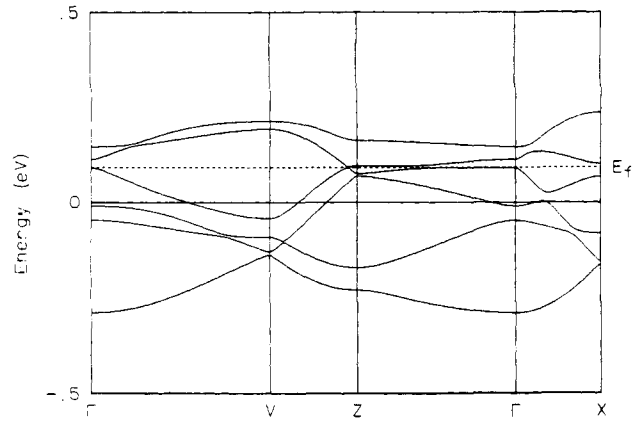

Figure 5. Calculated band structure of I.

the transfer integrals t between the HOMO of pairs of neighboring molecules evaluated using the dimer-splitting approximation[31]

$$t = \langle \mathrm{HOMO}_1 | \mathcal{H} | \mathrm{HOMO}_2 \rangle$$

where $\mathcal{H}$ is the EHT effective Hamiltonian. The parameters used in the present work were set equal to those used in calculations on the Bechgaard salts using the same approximations. The transfer integrals are labeled in Figure 3, and the values are included in Table II.

The largest overlaps are found along the a direction (AB2, AB4, BB3 ~ 100 meV); they are negative for the a–c direction (AB1, AB3, BB1) (see Figure 3), which corresponds to the side-by-side arrangement of the dimers, with absolute values that represent between 30 and 40% of t_a. In contrast, they are small (20% of t_a) or zero in the stack along the c direction. These results may be compared to the overlap integrals calculated by Mori[13d] for $(BEDT\text{-}TTF)_3Cl_2\cdot 2H_2O$, a material which exhibits the same charge stoichiometry and packing motifs. In the latter, the ratio of the negative to the positive overlaps is increased to 67%, and there are no zero interactions along the stacks. It is possible that the different ratios of negative to positive overlaps are model dependent. However, the intrastack transfer integrals should be more closely related to the structures: in particular, the three translationally inequivalent molecules in each unit cell belong to the same stack in the chloride salt but to neighboring stacks in the present case.

The calculated band structure of I is shown in Figure 5. The Fermi energy (E_F = 90 meV) is determined by assuming a $^2/_3+$ average charge per molecule, as discussed above. The four lower bands are almost completely filled so that the Fermi surface comprises very small pockets of electrons and holes. The results predict that I should be a semi-metal, but because of the approximations involved in the calculation, slight changes in the transfer integrals could lead either to a more conducting metal or to a semiconductor. It should be noted that the bands close to the Fermi level along the Γ–Z direction are extremely flat, so that minor modification of the structure and/or the stoichiometry would reinforce the semimetallic character.

Electrical-Transport Properties. The room-temperature conductivity of $(BEDT\text{-}TTF)_3CuCl_4\cdot H_2O$ shows an anisotropy of 7:1 within the layer; that is, $\sigma_{RT} \parallel a$–c is 140 (20) S cm^{-1} and $\sigma_{RT} \perp a$–c is 20 (2) S cm^{-1}, with only minor variation between samples. Some crystals show metallic conductivity down to very low temperatures (200 mK in one case), while some show a minimum in resistivity below 50 K. All the crystals studied show a broad maximum in resistance above 200 K (Figure 6a). The ratio of the maximum resistance to that at room temperature is at most 2, and the resistance of the purely metallic crystals at 4 K to that at room temperature is a maximum of 100. Pressure measurements of the resistance up to 12 kbar were possible down to 2 K; in those temperature and pressure regions, no superconductivity was observed. Our results confirm those of Shibaeva et al.[6]

The thermopower of $(BEDT\text{-}TTF)_3CuCl_4\cdot H_2O$ along the a–c direction is shown in Figure 6b. It increases to a maximum of

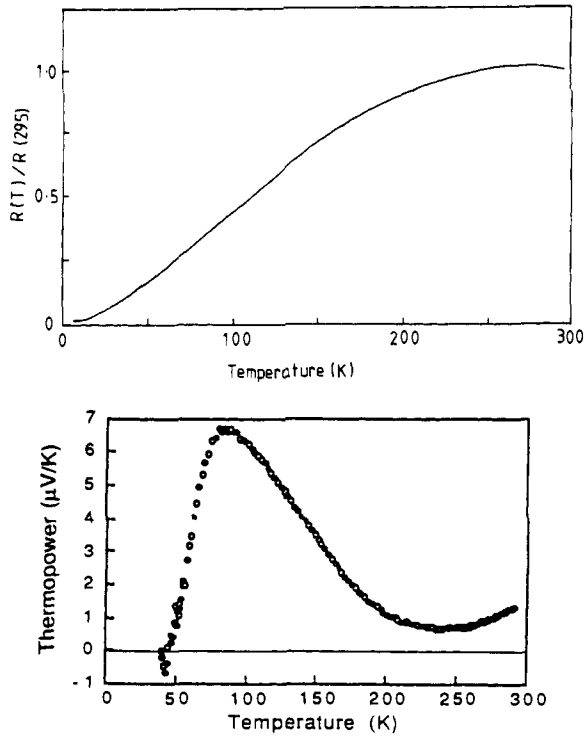

Figure 6. (a, Top) Temperature dependence of the resistivity of I at 3 kbar. (b, Bottom) Thermopower versus temperature for I.

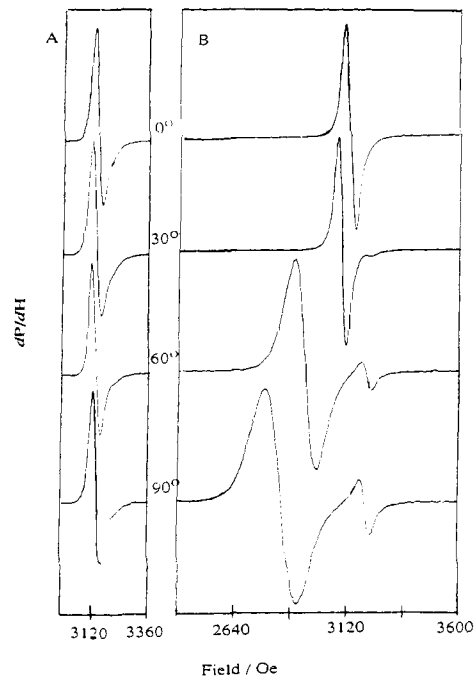

Figure 7. EPR spectra of I at 35 K showing the orientation dependence of the line shape and the overlap of the conduction and the Cu electron resonances: ω rotation about b^*; (B) θ rotation about a–c.

7 μV/K at ~80 K and drops to ~1 μV/K between 200 and 300 K. The small value of the thermopower is consistent with the metallic behavior. The temperature variation is probably the result of competition between electrons and holes as majority charge carriers.

Electron Paramagnetic Properties. The EPR spectra of $(BEDT\text{-}TTF)_3CuCl_4\cdot H_2O$ are characterized by two Lorentzian signals at $g \sim 2$ (Figure 7). The g value and line shape and width of the strong line depend on the orientation of the crystal with respect to the static magnetic field (H_0) and the microwave oscillating field (H_1), and for the weak signal, the dependence of these parameters can only be measured for a limited angular region

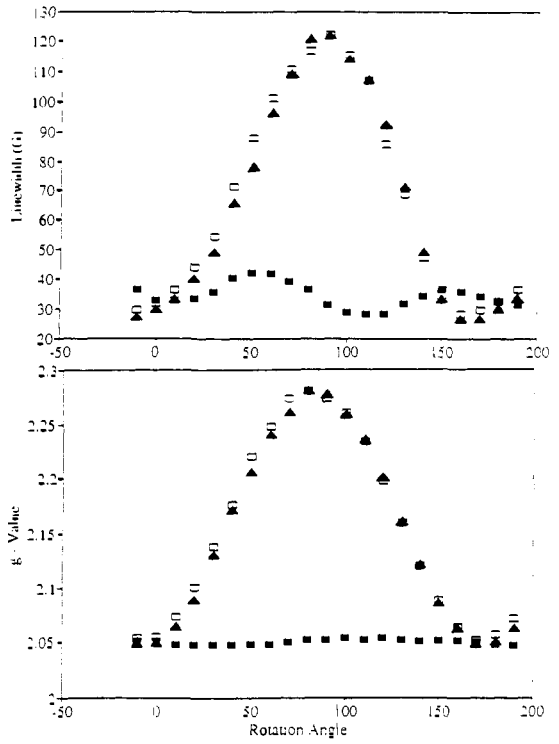

Figure 8. Angular dependence of the line width and g value of the cu resonance of I at 35 K: triangle, θ rotation; empty square, ϕ rotation; filled square, ω rotation.

due to the strong overlap of the two signals. However, it is clear that the g value of the weak signal is less sensitive to the orientation of the crystal. The dependence of the EPR spectra on microwave power was measured in the range 0.1–100 mW at a modulation frequency of 100 kHz in order to check for saturation effects. The intensities of the lines were found to be linear in the square of the power at both 300 and 35 K, indicating no saturation effects. The line shape, that is, the asymmetry A/B (the ratio of the positive to the negative part of the first derivative of the power with respect to the field) of the Dysonian line,[18] was found to be independent of the microwave power. This validates the application of Feher–Kip procedure for the line shape analysis for a flat-plate geometry sample.[19] The following experiments were performed: (i) the angular dependence of the line width, g value, spin susceptibility, and microwave conductivity at room temperature and at 35 K, for the crystal orientation shown in Figure 1; (ii) temperature dependence of the above observables for four different orientations.

At room temperature, the lines are so wide that the two resonances cannot be separated, but at 35 K, they are sufficiently narrow to permit independent fitting of each. The g values and line widths are shown in Figure 8 and are compared with those of the mixed-valence (BEDT-TTF)$_6$[Cu^{II}Cl$_2$Br$_2$][Cu^{I}Br$_2$] and (BEDT-TTF)$_6$[Cu^{II}Br$_4$][Cu^{I}Br$_2$] salts (Table III). The g value of the stronger line varies from 2.05 to 2.29 when the crystal is rotated about the pseudo-4-fold axis of the $CuCl_4$ ion with the static field perpendicular to this axis, while it remains constant at 2.05 for rotation along the 4-fold axis. These values are within the range for isolated Jahn-Teller distorted $CuCl_4^{2-}$ ions in the solid state.[27b] If we assume that the anions show axial symmetry, the calculated molecular g values are $g_\parallel = 2.28$ and $g_\perp = 2.05$ by fitting the observed g values to

$$g_{obs}^2 = g_\parallel^2 \cos^2(\theta + \pi/2) + g_\perp \sin^2(\theta + \pi/2)$$

The line widths vary from 30 to 120 G according to $31.6[1 + 3\cos^2(\theta + \pi/2)]$ for θ and ϕ rotation and $28 + 2[1 + 3\cos^2(2\theta + \pi/2)]$ for ω rotation.

The g value of the weak line is almost constant (2.03–2.05) with the angle. The angular dependences of the g value and line width of the strong signal are both consistent with those of Cu^{II} salts.

Table III. g Values and EPR Line Widths of Copper Halide Salts of BEDT-TTF

compound	g value min	g value max	H_{pp}/G min	H_{pp}/G max	θ/K
(BEDT-TTF)$_3$CuCl$_4$·H$_2$O					
Cu electron	2.05	2.25	44	150	~+1
cond electron	2.03	2.04	40	60	
(BEDT-TTF)$_2$CuCl$_4$					
Cu electron	2.05	2.30	25	66	~0
(BEDT-TTF)$_3$CuBr$_3$[a]					
>60 K	2.02	2.065	115	135	−107
<60 K	2.04	2.11	37	60	
(BEDT-TTF)$_3$CuClBr$_2$[a]					
>60 K	2.02	2.08	90	100	−61
<60 K	2.037	2.16	90	100	

[a] Reference 23a,c. The signals from Cu electrons and conduction electrons in these two compounds are not separable at all angles and temperatures studied.

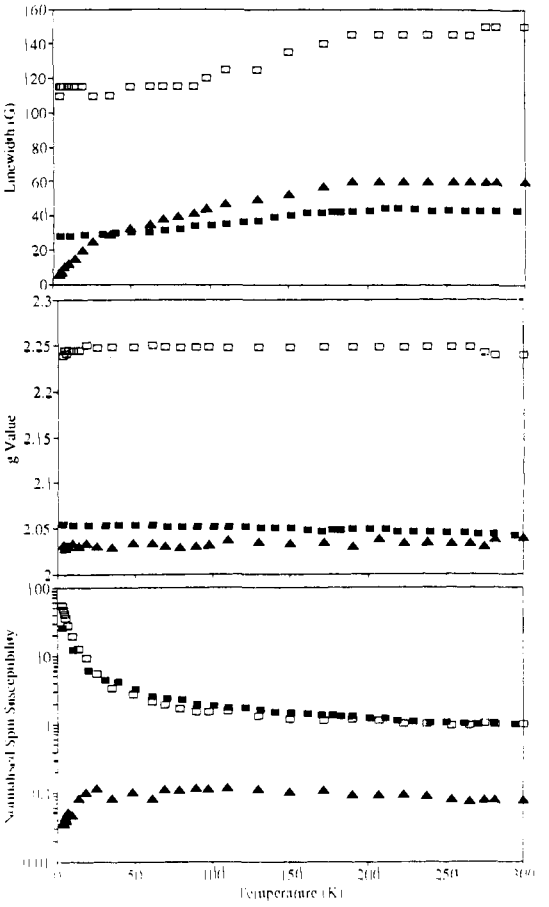

Figure 9. Temperature dependence of the normalized spin susceptibility, line width, and g value of the Cu ($H \parallel a$–c, empty square; $H \parallel b^*$, filled square) and conduction ($H \parallel a$–c, triangle) electron resonances of I.

Thus, we assign the intense line to the localized moments (i.e. Cu) and the weak one to BEDT-TTF conduction electrons. The angular dependence of the microwave conductivity is not precisely determined due to the irregular shape of the small crystals used. However, the derived conductivities parallel and perpendicular to the needle axis (a–c) of the crystals at 300 K (137/17 S cm^{-1}) are quite consistent with those measured at 15 Hz and dc (140/20 S cm^{-1}).

The temperature dependences of the line width, g value, and normalized spin susceptibility are shown in Figure 9. The line widths of both signals decrease as the temperature is lowered: that of Cu from 150 to 115 G for $H_0 \parallel a$–c and from 40 to 28 G for $H_0 \parallel b^*$ and that of the conduction electrons from 60 to 5 G for $H_0 \parallel a$–c. The relative change of the line widths with temperature reinforces the conclusion that the strong and weak signals are the

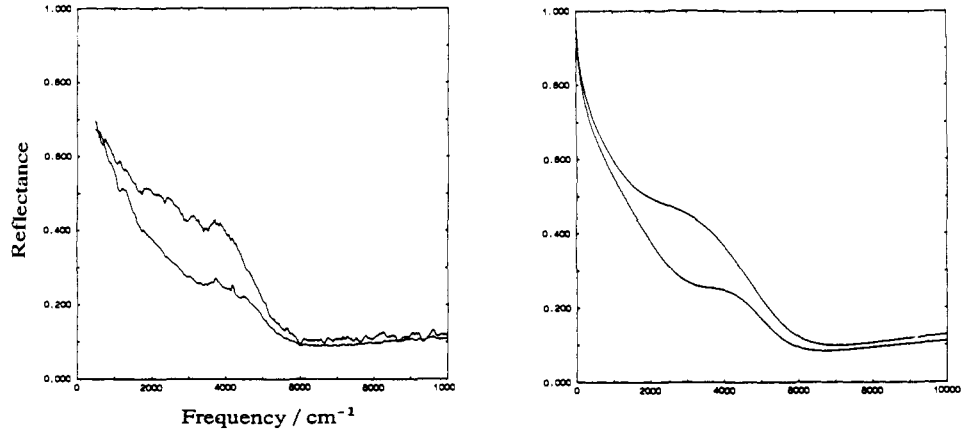

Figure 10. Reflectivity of I for $E \parallel a$–c and $E \perp a$–c. The solid line is a Drude–Lorentz fit to the data.

Cu and the free-carrier resonances, respectively. For example, the line width of conduction electron resonance in the organic superconductor β-(BEDT-TTF)$_2$AuI$_2$[34] decreases from 16 to 2 G on lowering the temperature from 300 to 4 K; in the conductor β''-(BEDT-TTF)$_2$AuBr$_2$,[20] it decreases from 60 to 0.3 G; and in the semiconductor β'-(BEDT-TTF)$_2$AuCl$_2$,[35] it decreases from 7 to 1 G. The susceptibility derived from the Cu resonance was found to increase on lowering temperature, and that of the conduction electron is temperature independent in the range 30–300 K, while below 30 K, it falls monotonically to 30% of the room-temperature value. The g value of the conduction-electron resonance remains constant within experimental accuracy over the temperature range studied. That of the Cu resonance decreases at a rate of 4×10^{-5} K^{-1}.

The temperature dependence of the microwave conductivity derived from analysis of the line shape of the spectra is orientation dependent. That along a–c shows an increase of 5-fold on lowering the temperature from 300 to 4 K, whereas that perpendicular to the a–c direction decreases by ~10% of the room-temperature value. The skin depth [$\delta_y = c/(2\pi\sigma_z\omega)^{1/2}$, where the microwave is propagating in the y direction, the oscillating electric field is along z, the oscillating magnetic field is along x, σ_z is the conductivity along z, and ω is the microwave frequency] is estimated to be 0.13 ($\parallel a$–c) and 0.05 mm ($\perp a$–c).[18,19] This temperature-dependent anisotropy of the conductivity may be responsible for the sample dependence seen in resistive measurements (since contact alignment on such small crystals can be very difficult).

Optical Properties. The reflectivities of two crystals of I were measured in the spectral range 400–30 000 cm^{-1}. Careful examination of the polarization dependence of the reflectivity indicate that the principal axes of the optical constants lie parallel and perpendicular to the a–c needle axis. Figure 10 shows the reflectance with the electric vector polarized parallel and perpendicular to this axis. No significant difference was observed between the two crystals. The reflectivity spectra are characterized by a peak at ca. 4000 cm^{-1} overlapping a Drude-like tail. Some very weak vibrational structures can also be observed.

The reflectivity was fitted in the region 400-20 000 cm^{-1}, using the Drude–Lorentz formula for the dielectric constant

$$\epsilon(\omega) = \epsilon_c - \omega_p^2/\omega(\omega + i\gamma) + \Omega_o^2/(\omega_o^2 - \omega^2 - i\omega\gamma_o)$$

where ϵ_c is the underlying core dielectric constant due to all higher energy processes, γ is the Drude relaxation rate, and ω_p is the unscreened plasma frequency. Ω_0, ω_o, and γ_o are respectively the oscillator strength, the frequency, and the width of the Lorentzian oscillator. As the absolute reflectivity was difficult to measure reliably, an additional scaling factor α was allowed for in fitting the reflectivity, i.e.

$$R(\omega) = \alpha(\epsilon(\omega)^{1/2} - 1)/(\epsilon(\omega)^{1/2} + 1)$$

The fit to the reflectivity is shown in Figure 10 using the fitting parameters listed in Table IV. In the same table are listed some effective band parameters derived from the Drude fit. For example, the optical effective mass is related to the plasma frequency by the relation

$$m^* = ne^2/(\epsilon_o\omega_p^2)$$

with n being the carrier density, while the transfer integral t is obtained from the tight-binding formula

$$4t = \pi\rho^2/(m^*d^2 \sin(\pi\rho/2))$$

where ρ is the number of carriers per molecule and d is the average intermolecular spacing.

Table IV. Parameters of the Drude–Lorentz Fit to and Band Parameters from the Optical Reflectivity of I

	$E \parallel a$–c	$E \perp a$–c
$\omega_p/10^3$ cm^{-1}	9.4	8.9
$\gamma/10^3$ cm^{-1}	2.71	3.38
ϵ_c	6.0	5.0
$\omega_o/10^3$ cm^{-1}	2.93	4.24
$\gamma_o/10^3$ cm^{-1}	3.52	2.48
$\Omega_o/10^3$ cm^{-1}	8.9	5.3
m^*_{opt}/m_e	1.25	1.5
$4t$/eV	0.24	0.66
d/Å	6.6	4.3
ρ	$^2/_3$+	
$(1/V_m)$/Å^3	600	

Discussion

The electrical properties of I can usefully be compared with those of other BEDT-TTF salts having 3:2 charge stoichiometry, and in particular the chloride salt. For example, the electrical conductivity of I is 3–5 times less than that of (BEDT-TTF)$_3$Cl$_2$·2H$_2$O,[13] in agreement with smaller transfer integrals (100 meV in I versus 160 meV in the latter[13d]). The conductivity anisotropies are identical in the two salts, with the larger component along the side-by-side contacts of the BEDT-TTF molecules. In the former case, this result does not correspond to the larger calculated transfer integrals which are t_a.

A much more important discrepancy between theory and experiment is the prediction from the band-structure calculations[13d] that both salts should be semi-metals, whereas at room temperature they both exhibit metallic conductivity. On the other hand, I is the only BEDT-TTF salt of 3:2 shoichiometry to remain metallic to very low temperatures at ambient pressure. In general, the 3:2 salts suffer a metal (or semi-metal) to insulator (or semiconductor) transition at low temperature. Some have sharp transitions [e.g. (BEDT-TTF)$_3$(ClO$_4$)$_2$],[21] and others have broad

(34) Talham, D. R.; Kurmoo, M.; Day, P.; Obertelli, D. S.; Parker, I. D.; Friend, R. H. *J. Phys. C: Solid State Phys.* **1986**, *19*, L383–388.
(35) Kurmoo, M.; Talham, D. R.; Day, P. In *Lower Dimensional Systems and Molecular Devices*; Metzger, R. M., Day, P., Papavassiliou, G., Eds.; NATO ASI Series B, Vol. 248; Plenum: New York, 1991; pp 169–173.

ones (e.g. (BEDT-TTF)$_3$Cl$_2$·2H$_2$O).[13] We have demonstrated that the transition in the chloride salt is accompanied by a gradual trimerization of the BEDT-TTF molecules within the chain.[13f] It is important to note that, in the latter, the three independent molecules belong to one stack while, for I, the corresponding molecules belong to two different stacks, so that trimerization in the same sense is not possible. The chloride is also the only example of a 3:2 salt in which the metal–insulator transition can be suppressed by pressure to stabilize a superconducting state.[13a]

The interaction between the localized moments and the conduction electrons in I is manifested in two ways:[36]

First, there is a shift in g value and broadening of the EPR line. The two conditions for strongly interacting systems are (i) the g value of the localized moments and that of the conduction electrons should be close to one another and (ii) the spin–lattice relaxation rate of the localized moments must be sufficiently small. Unfortunately, for such a molecular system, the g value as well as the line width is very dependent on the geometry adopted by the ions, and in the absence of data on the g values and spin–lattice relaxation rates of an isolated ion, no estimate can be made. The fact that we observe two signals for the two spin sublattices indicates that we are not in a "bottleneck" regime and the exchange interaction is small. Should exchange be present, the temperature dependence of the g value should scale the change in susceptibility by

$$g_{obs} = (g_e\chi_e + g_i\chi_i)/(\chi_e + \chi_i) \sim g_0 + bT$$
$$\chi_i = C/(T - \Theta)$$

where e is for conduction electrons and i for localized moments. Our results fit a g_0 ($H_0 \parallel b^*$) value of 2.052 and b of -4×10^{-5} K^{-1}. The g value is distinctly larger than those found in β- or α'-phase BEDT-TTF salts (2.003–2.010),[12,34] which strongly suggests that there is interaction between the two spin systems.

A second indication of interaction between localized and conduction electrons in the fall in χ_e from its Pauli limit as the χ_i increases at low temperature (Figure 9). Most striking of all, however, on plotting $(\chi - \chi_0)T$ versus T for the Cu resonance, one observes a gradual increase at low temperature, indicating short-range ferromagnetic interaction. Fits to the data for the Cu resonance using a simple Curie–Weiss law and a Bleaney–Bowers[37] model for a dimer give a positive ferromagnetic temperature factor of 1 (1) and 4 (1) K, respectively. However, detailed bulk susceptibility measurements at very low temperatures will be needed to confirm the EPR data. Such measurements need a greater quantity of crystals, which have to be individually selected due to the polymorphism. It should be borne in mind that the Cu–Cu distances are at least 8.5 Å, so direct exchange interaction between the Cu atoms will be very small. On the other hand, the $CuCl_4^{2-}$ groups are arranged in dimeric units bridged by H_2O molecules, which may provide an exchange pathway. Nor can we rule out the possibility of exchange between the Cu atoms via the free carriers of the conducting BEDT-TTF layers.

There may be several reasons for not observing superconductivity in I. Whether it is due to a small amount of chloride impurity or whether it is the effect of introducing a magnetic anion into the lattice is not known. Further work will be needed to decide this point.

Conclusion

The compound (BEDT-TTF)$_3$CuCl$_4$·H$_2$O described in this paper is the first example of a conducting charge-transfer salt of the BEDT-TTF series containing a magnetic anion to be fully characterized both structurally and electronically. The crystal structure consists of alternating layers of organic cations and inorganic anions, the former consisting of side-by-side stacks of BEDT-TTF, each bearing the same charge of $^2/_3$+, though with three crystallographically inequivalent molecules per unit cell. The $CuCl_4^{2-}$ anions, with strongly flattened tetrahedral geometry, are linked together by pairs of H_2O molecules to form dimers. (BEDT-TTF)$_3$CuCl$_4$·H$_2$O provides the first instance in which spin resonance due to both localized and conduction electrons has been observed in the BEDT-TTF class of compounds. While it is metallic from room temperature down to 200 mK, there is no transition to a superconducting state. The EPR g values and line widths give evidence for a weak interaction between the spin systems of the organic and inorganic parts of the structure, and at low temperature, there is a small positive deviation of χ(Cu)T, suggesting weak short-range ferromagnetic spin correlations, probably of intradimer type. It remains to be seen whether the absence of superconductivity is the result of these correlations. We are continuing our efforts to synthesize other molecular charge-transfer salts designed to investigate the possible coexistence of superconductivity and magnetic order in a molecular lattice.

Acknowledgment. We thank the SERC (U.K.), CNRS (France), and NATO for partial support of this work.

Supplementary Material Available: Figures showing the labeling scheme of atoms and tables of atomic coordinates, bond lengths and angles, and thermal parameters (9 pages); a listing of calculated and observed structure factors (46 pages). Ordering information is given on any current masthead page.

(36) (a) Barnes, S. E. *Adv. Phys.* **1980**, *30*, 801–938. (b) Odermatt, R. *Helv. Phys. Acta* **1981**, *54*, 1–84.

(37) (a) Bleaney, B.; Bowers, K. D. *Proc. R. Soc. London, A* **1952**, *214*, 451–465. (b) Kato, M.; Muto, Y. *Coord. Chem. Rev.* **1988**, *92*, 45–83.